Inorganic Chemistry
Article

Inorg. Chem. 2010, 49, 1245–1251 1245
DOI: 10.1021/ic9022213

Synthesis and Properties of N_7O^+

Karl O. Christe,*,† Ralf Haiges,† William W. Wilson,† and Jerry A. Boatz‡

†*Loker Research Institute and Department of Chemistry, University of Southern California, Los Angeles, California 90089-1661 and* ‡*Air Force Research Laboratory, Edwards Air Force Base, California 93524*

Received November 10, 2009

The reaction of $NOF_2^+SbF_6^-$ with an equimolar amount of HN_3 in an anhydrous HF solution at −45 °C produces $N_3NOF^+SbF_6^-$. When an excess of HN_3 is used in this reaction, $N_7O^+SbF_6^-$ is formed. However, this compound could not be isolated as a solid and rapidly decomposed in a quantitative manner with N_2O evolution to $N_5^+SbF_6^-$. This reaction represents a novel and more convenient synthesis for $N_5^+SbF_6^-$ because $NOF_2^+SbF_6^-$ is more readily accessible than $N_2F^+SbF_6^-$ and the N_5^+ can be labeled in all five positions with ^{15}N by the simple use of terminally singly labeled N_3^-. The formation of the N_7O^+ cation was established by isotopic labeling experiments and theoretical calculations. It is shown that the addition of a second azido ligand to the same central atom allows the attack of the negatively charged Nα atom of one ligand by the positively charged Nγ atom of the second ligand, thereby greatly lowering the activation energy barrier toward decomposition and explaining why geminal diazides are much less stable than either monoazides or vicinal diazides.

Introduction

An area of particular interest for energetic materials is high-nitrogen chemistry. In high-nitrogen chemistry, most of the energy release stems from the fact that N−N single bonds (average bond energy ∼159 kJ/mol) and N=N double bonds (average bond energy ∼419 kJ/mol) are considerably weaker than one-third or two-thirds of the N≡N triple-bond energy in dinitrogen (bond energy of 946 kJ/mol). Therefore, polynitrogen compounds possess large positive heats of formation and decompose exothermically with the liberation of large amounts of N_2. The formation of large amounts of N_2 in the decomposition products is highly desirable for applications such as gun propellants where the smoke, flame temperature, and the corrosion of the gun barrels are greatly reduced by the N_2. During the past decade, major breakthroughs in this field have been achieved by the syntheses and identification of several novel ions, the V-shaped N_5^+ cation,[1,2] the N_3NOF^+ cation both as a *z* and *e* isomer,[3] and the *cyclo*-N_5^- anion.[4] The chemistry of N_5^+ and N_5^- has been highlighted by us in a recent review paper.[5] The synthesis and characterization of N_3NOF^+ has also been described already in detail,[3] and here the synthesis of the N_7O^+ cation is reported. In particular, the question of why N_7O^+ is thermally so much less stable than N_3NOF^+ is addressed and whether this instability is innate to geminal diazides.

Experimental Section

Caution! *Neat HN_3 is highly explosive and should, whenever possible, be handled only in solution. Anhydrous HF can cause severe burns, and contact with the skin must be avoided.*

Materials and Apparatus. All reactions were carried out in Teflon-FEP ampules that were closed by stainless steel valves. Volatile materials were handled in a stainless steel/Teflon-FEP vacuum line.[6] All reaction vessels and the vacuum line were passivated with ClF_3 prior to use. Nonvolatile materials were handled in the dry argon atmosphere of a glovebox.

Raman spectra were recorded in the Teflon reactors in the range 4000−80 cm^{-1} on a Bruker Equinox 55 FT-RA spectrophotometer, using a Nd:YAG laser at 1064 nm or a Cary Model 83GT spectrometer using the 488 nm line of an Ar-ion laser. The ^{14}N NMR spectra were recorded in anhydrous HF as a solvent on a Bruker AMX-500 NMR instrument at 36.13 MHz using a 5 mm broad band probe. Neat CH_3NO_2 ($\delta = 0$ ppm), measured at room temperature, was used as an external standard.

The starting materials, $NOF_2^+SbF_6^-$[7] and HN_3[2], were prepared according to literature methods. HF was dried by storage over BiF_5[8] or TaF_5.

Reaction of $NOF_2^+SbF_6^-$ with HN_3. In a typical experiment, $NOF_2^+SbF_6^-$ (0.3 mmol) was added to a prepassivated, thin-walled,

*To whom correspondence should be addressed. E-mail: kchriste@usc.edu.

(1) Christe, K. O.; Wilson, W. W.; Sheehy, J. A.; Boatz, J. A. *Angew. Chem., Int. Ed.* **1999**, *38*, 2004.
(2) Vij, A.; Wilson, W. W.; Vij, V.; Tham, F. S.; Sheehy, J. A.; Christe, K. O. *J. Am. Chem. Soc.* **2001**, *123*, 6308.
(3) Wilson, W. W.; Haiges, R.; Boatz, J. A.; Christe, K. O. *Angew. Chem., Int. Ed.* **2007**, *46*, 3023.
(4) Vij, A.; Pavlovich, J. G.; Wilson, W. W.; Vij, V.; Christe, K. O. *Angew. Chem., Int. Ed.* **2002**, *41*, 3051.
(5) Christe, K. O. *Propellants, Explos., Pyrotech.* **2007**, *32*, 194.
(6) Christe, K. O.; Wilson, W. W.; Schack, C. J.; Wilson, R. D. *Inorg. Synth.* **1986**, *24*, 39.
(7) Christe, K. O. *J. Am. Chem. Soc.* **1995**, *117*, 6136.
(8) Christe, K. O.; Wilson, W. W.; Schack, C. J. *J. Fluorine. Chem.* **1978**, *11*, 71.

Published on Web 01/07/2010

4 mm o.d. FEP ampule, which was closed by a stainless steel valve. On the vacuum line, anhydrous HF (270 mg) was condensed in at −196 °C, and the $NF_2O^+SbF_6^-$ was dissolved in the HF at room temperature. The ampule was cooled back to −196 °C, and a mixture of HN_3 (0.3 or 0.6 mmol) and HF (750 or 1500 mg, respectively) was condensed in. The FEP ampule was heat-sealed and warmed to −80 °C. It was then inserted into a standard 5 mm o.d. glass NMR tube and quickly transferred into the probe of the NMR spectrometer. The sample was warmed to ambient temperature in steps of 10 °C and monitored by NMR spectroscopy.

Theoretical Methods. The molecular structures, harmonic vibrational frequencies, and infrared and Raman vibrational intensities were calculated using (a) second-order perturbation theory (MP2, also known as MBPT(2)[9]) and the 6-311G(2df) basis set,[10] denoted as MP2/6-311G(2df), (b) MP2 with the correlation consistent polarized valence triple-ζ basis set,[11] that is, MP2/cc-pvtz, and (c) density functional theory methods using the B3LYP hybrid functional,[12] which included the VWN5 correlation functional[13] and the 6-311G(2df) basis set (B3LYP/6-311G(2df)). In addition, the structure and harmonic vibrational frequencies of the C_{2v} isomer of N_7O^+ were computed using the coupled cluster singles plus doubles with a perturbative estimate of triples (CCSD(T)[14]) method, with the 6-31G(d) basis set.[15] Hessians (energy second derivatives) were calculated for all stationary points to verify them as either local minima or transition states (i.e., having zero or one negative eigenvalue of the Hessian, respectively). Intrinsic reaction coordinate[16] traces were generated using the Gonzales−Schlegel second-order method.[17] The relative energies of all stationary points were refined by performing "completely renormalized" CR-CCSD(T)[18] single-point energy computations at the MP2/6-311G(2df) geometries. B3LYP/6-311G(2df) (MP2/6-311G(2df)) zero-point vibrational energy corrections were scaled by 0.9806 (0.9748).[19] The calculations were performed using the electronic structure codes GAMESS,[20] Gaussian 03,[21] and ACES II.[22] The second derivatives were analyzed by using the program BMATRIX.[23]

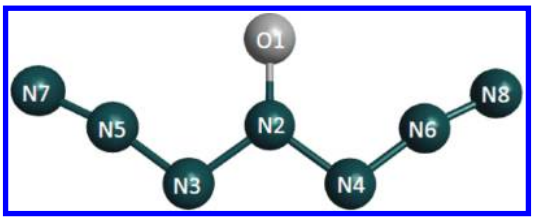

Figure 1. Minimum-energy structure (bond distances in Å, angles in deg) of the C_{2v} isomer of N_7O^+ calculated at the MP2/cc-pvtz level with CCSD(T)/6-31G(d) values given in parentheses: O1−N2, 1.216 (1.221); N2−N3, 1.353 (1.371); N3−N5, 1.293 (1.320); N5−N7, 1.130 (1.131); O1−N2−N3, 126.2 (126.3); N2−N3−N5, 107.7 (106.9); N3−N5−N7, 170.6 (168.8); N2−N3−N5−N7, 180.0 (180.0). Weinhold's NBO charges at the PBE1PBE/6-311+G(2df) level: O, −0.25; N2, 0.46; N3, −0.13; N5, 0.23; N7, 0.29.

Results and Discussion

Chemical Synthesis. In the synthesis of N_5^+,[1,2] N_2F^+ was reacted with HN_3 to replace the F atom by an azido group. A similar approach was applied to the well-known NOF_2^+ cation,[7,24−29] and when a stoichiometric amount of HN_3 was used, formation of the N_3NOF^+ cation resulted. The $N_3NOF^+SbF_6^-$ salt was found to be marginally stable at ambient temperature,[3] and therefore, an obvious challenge was to explore whether the second F atom could also be replaced by an azido group and, thus, provide a synthesis for the novel N_7O^+ cation (eq 1).

$$N_3NOF^+SbF_6^- + HN_3 \xrightarrow{aHF} N_7O^+\,SbF_6^- + HF \quad (1)$$

The replacement of F by N_3 started to proceed at temperatures as low as −64 °C, and when stoichiometric amounts of $NOF_2^+SbF_6^-$ and HN_3 were used, $N_3NOF^+SbF_6^-$ was formed in high yield and could be isolated by pumping off the solvent and gaseous products at low temperatures. With an excess of HN_3, replacement of the second fluorine atom started to occur in the same temperature range; however, the expected N_7O^+ cation could neither be directly observed by low-temperature NMR spectroscopy nor be isolated in the form of its SbF_6^- salt. Instead, N_2O gas evolution and quantitative formation of $N_5^+SbF_6^-$[2] were observed (eq 2).

$$NOF_2^+\,SbF_6^- + 2HN_3 \xrightarrow{aHF} N_5^+SbF_6^- + 2HF + N_2O \quad (2)$$

Since the $NOF_2^+SbF_6^-$ is more readily accessible[8] than $N_2F^+SbF_6^-$, reaction 2 represents a more convenient and novel synthesis of $N_5^+SbF_6^-$.

(9) (a) Moller, C.; Plesset, M. S. *Phys. Rev.* **1934**, *46*, 618. (b) Pople, J. A.; Binkley, J. S.; Seeger, R. *Int. J. Quantum Chem.* **1976**, *S10*, 1. (c) Frisch, M. J.; Head-Gordon, M.; Pople, J. A. *Chem.Phys.Lett.* **1990**, *166*, 275. (d) Bartlett, J.; Silver, D. M. *Int. J. Quantum Chem. Symp.* **1975**, *9*, 1927.
(10) (a) Krishnan, R.; Binkley, J. S.; Seeger; Pople, J. A. *J. Chem. Phys.* **1980**, *72*, 650. (b) Frisch, M. J.; Pople, J. A.; Binkley, J. S. *J. Chem. Phys.* **1984**, *80*, 3265.
(11) Dunning, T. H., Jr. *J. Chem. Phys.* **1989**, *90*, 1007.
(12) (a) Becke, A. D. *J. Chem. Phys.* **1993**, *98*, 5648. (b) Stephens, P. J.; Devlin, F. J.; Chablowski, C. F.; Frisch, M. J. *J. Phys. Chem.* **1994**, *98*, 11623. (c) Hertwig, R. H.; Koch, W. *Chem. Phys. Lett.* **1997**, *268*, 345.
(13) Vosko, S. H.; Wilk, L.; Nusair, M. *Can. J. Phys.* **1980**, *58*, 1200.
(14) Purvis, G. D., III; Bartlett, R. J. *J. Chem. Phys.* **1982**, *76*, 1910.
(15) (a) Hehre, W. J.; Ditchfield, R.; Pople, J. A. *J. Chem. Phys.* **1972**, *56*, 2257. (b) Hariharan, P. C.; Pople, J. A. *Theor. Chim. Acta* **1973**, *28*, 213.
(16) Ishida, K.; Morokuma, K.; Komornicki, A. *J. Chem. Phys.* **1977**, *66*, 2153.
(17) Gonzales, C.; Schlegel, H. B. *J. Chem. Phys.* **1989**, *90*, 2154.
(18) (a) Piecuch, P.; Kucharski, S. A.; Kowalski, K.; Musial, M. *Comput. Phys. Commun.* **2002**, *149*, 71. (b) Kowalski, K.; Piecuch, P. *J. Chem. Phys.* **2000**, *113*, 18. (c) Kowalski, K.; Piecuch, P. *J. Chem. Phys.* **2000**, *113*, 5644.
(19) Scott, A. P.; Radom, L. *J. Phys. Chem.* **1996**, *100*, 16502.
(20) Schmidt, M. W.; Baldridge, K. K.; Boatz, J. A.; Elbert, S. T.; Gordon, M. S.; Jensen, J. H.; Koseki, S.; Matsunaga, N.; Nguyen, K. A.; Su, S. J.; Windus, T. L.; Dupuis, M.; Montgomery, J. A. *J. Comput. Chem.* **1993**, *14*, 1347.
(21) Frisch, M. J., et al. *Gaussian 03*, revision D.01; Gaussian, Inc.: Wallingford, CT, 2004.
(22) Stanton, J. F.; Gauss, J.; Watts, J. D.; Nooijen, M.; Oliphant, N.; Perera, S. A.; Szalay, P. G.; Lauderdale, W. J.; Gwaltney, S. R.; Beck, S.; Balkova, A.; Bernholdt, D. E.; Baeck, K. K.; Rozyczko, P.; Sekino, H.; Hober, C.; Bartlett, R. J. *ACES II, Quantum Theory Project*; University of Florida: Gainesville, FL. Integral packages included are VMOL (Almlof, J.; Taylor, P. R.), BPROPS (Taylor, P. R.), and ABACUS (Helgaker, T.; Jensen, A. H. J.; Jorgensen, P.; Olsen, J.; Taylor, P. R.).
(23) Komornicki, A. *BMATRIX*, version 2.0; Polyatomics Research Institute: Palo Alto, CA, 1996.
(24) Fox, W. B.; MacKenzie, J. S.; Vanderkooi, N.; Sukorkik, B.; Wamser, C. A.; Holmes, J. R.; Eibeck, R. E.; Stewart, B. B. *J. Am. Chem. Soc.* **1966**, *88*, 2604.
(25) Christe, K. O.; Maya, W. *Inorg. Chem.* **1969**, *8*, 1253.
(26) Wamser, C. A.; Fox, W. B.; Sukornik, B.; Holmes, J. R.; Stewart, B. B.; Juurick, R.; Vanderkooi, N.; Gould, D. *Inorg. Chem.* **1969**, *8*, 1249.
(27) Christe, K. O.; Hon, J. F.; Pilipovich, D. *Inorg. Chem.* **1973**, *12*, 84.
(28) Mason, J.; Christe, K. O. *Inorg. Chem.* **1983**, *22*, 1849.
(29) Vij, A.; Zhang, X.; Christe, K. O. *Inorg. Chem.* **2001**, *40*, 416.

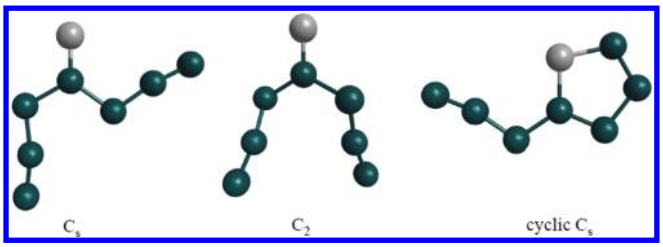

Figure 2. Higher-energy, local minima structures for N_7O^+. Oxygen (nitrogen) atoms are shown as light (dark) circles.

Equations 1 and 2 represent an oversimplification of all of the processes occurring in the $NOF_2^+/HN_3/HF$ system. NMR studies provided evidence for the presence and active participation of several equilibria. For example, at temperatures below −43 °C in HF solution, HN_3 can displace NOF_3 from its $NOF_2^+SbF_6^-$ salt due to the fact that $H_2N_3^+SbF_6^-$ is practically insoluble in HF at low temperatures (eq 3).

$$NOF_2^+SbF_6^- + HN_3 + HF \xrightarrow{aHF} H_2N_3^+SbF_6^-\downarrow + NOF_3 \quad (3)$$

At −43 °C, the NOF_3 is being consumed and N_3NOF^+ is formed. It is not clear whether the NOF_3 or NOF_2^+ is the reacting species, but generally NOF_2^+ is much more reactive than NOF_3.[7,24−29] At this temperature, N_3NOF^+ does not appear to react to an appreciable extent with HN_3, which, in the HF solution, is present in its protonated form, $H_2N_3^+HF_2^-$(nHF). When the temperature is raised to −33 °C, the second mole of HN_3 starts to enter the reaction, all of the NOF_3 is consumed, and N_5^+ and N_2O are formed. Although ^{15}N labeling experiments (see below) show that the N_5^+ originates from an intermediate N_7O^+, the N_7O^+ is not observable in the NMR spectra, indicating that its decomposition to N_5^+ and N_2O (eq 4) is more rapid than its formation.

$$N_7O^+SbF_6^- \rightarrow N_5^+SbF_6^- + N_2O \quad (4)$$

It should be pointed out that protonated HN_3 in HF solution, that is, $H_2N_3^+HF_2^-$(nHF), is less reactive toward NOF_2^+ than is HN_3, requiring several days at room temperature to form N_3NOF^+, N_5^+, and N_2O. This is not surprising because, due to their positive charges, the two cations should repel each other and not come in close enough contact for entering a reaction. The only reaction taking place would be through their equilibria with the neutral species.

Variation of the solvent (use of $(CF_3)_2CFH$) or the azide source (use of $(CH_3)_3SiN_3$) did not influence the outcome of these reactions. Obviously, the thermal stability of N_7O^+ must be significantly lower than that of N_3NOF^+, thus pre-empting its direct observation and isolation. Because the N_7O^+ cation could not be directly observed, a theoretical study was carried out, and its conclusions were experimentally corroborated by isotopic labeling experiments.

Theoretical Studies. On the basis of the known structure of N_3NOF^+[3] and the reaction leading to its formation, the most probable structure for N_7O^+ is the C_{2v} structure shown in Figure 1.

Table 1. Harmonic Vibrational Frequencies (cm^{-1}), Infrared Intensities (km/mol), and Raman Intensities ($Å^4$/amu) of C_{2v} N_7O^+

	B3LYP(5)/cc-pvtz	MP2/cc-pvtz	CCSD(T)/6-31G(d)
a_1 ν_1	2314 (12) [460]	2194 (9.3) [529]	2234 (6.2)
ν_2	1559 (153) [14]	1630 (85) [31]	1574 (104)
ν_3	1176 (0.4) [12]	1194 (4.7) [29]	1110 (0.3)
ν_4	968 (3.7) [7.6]	995 (1.6) [16.0]	969 (0.3)
ν_5	525 (2.5) [13]	543 (1.0) [17]	503 (3.6)
ν_6	427 (1.9) [2.3]	431 (1.8) [2.0]	411 (0.8)
ν_7	134 (0.01) [6.7]	131 (0.02) [8.3]	129 (0.1)
a_2 ν_8	504 (0) [2.0]	475 (0) [1.2]	452 (0)
ν_9	166 (0) [0.2]	161 (0) [0.005]	140 (0)
b_1 ν_{10}	703 (9.3) [0.15]	712 (6.3) [0.3]	687 (10)
ν_{11}	540 (6.1) [0.02]	511 (4.1) [0.04]	498 (4.8)
ν_{12}	94 (1.0) [0.08]	97 (1.1) [0.04]	93 (1.8)
b_2 ν_{13}	2307 (276) [40]	2182 (383) [61]	2222 (288)
ν_{14}	1220 (1069) [3.1]	1323 (1431) [5.9]	1219 (1281)
ν_{15}	1008 (70) [0.1]	1015 (116) [2.7]	933 (220)
ν_{16}	798 (10) [1.2]	835 (7.4) [1.8]	794 (43)
ν_{17}	495 (0.1) [0.02]	501 (1.4)[0.06]	478 (0.03)
ν_{18}	225 (2.8) [1.5]	221 (1.6) [0.6]	215 (2.8)

This structure was confirmed as the energy minimum by theoretical calculations at the B3LYP/6-311G(2df), MP2/6-311G(2df), MP2/cc-pvtz, and CCSD(T)/6-31G-(d) levels of theory. Other possible isomers have C_s and C_2 symmetry and a cyclic C_s structure (Figure 2) and are higher in energy than the C_{2v} structure by 2.6, 17.8, and 27.8 kcal/mol, respectively, at the B3LYP/6-311G(2df) level of theory. The relatively small energy difference of 3 kcal/mol between the C_{2v} and C_s structures shows that the N_3 arm in N_7O^+ is quite floppy and can very easily be rotated, an important aspect to remember when potential mechanisms for the N_2O elimination from N_7O^+ are discussed.

The calculated vibrational frequencies and infrared and Raman intensities are summarized in Table 1. As can be seen from the table, the calculated frequencies are somewhat method-dependent. Since in a catenated species consisting of several nearly linear groups of atoms with identical or similar masses, strong coupling of the vibrational modes must be expected, a normal coordinate analysis was also carried out for N_7O^+ at the B3LYP level. The results from this NCA are summarized in Table 2. The potential energy distribution shows that in most cases the normal vibrations are not highly characteristic and contain contributions from several symmetry coordinates, making many mode descriptions difficult; however, some assignments can be made. The dominant Raman mode, ν_1, at 2314 cm^{-1} and the strong IR mode, ν_{13}, at 2307 cm^{-1} are predominantly due to the in-phase and out-of-phase coupled stretching modes, respectively, of the two terminal N−N bonds. The 1559 cm^{-1} vibration, ν_2, is 51% stretching of the N−O bond, and the dominant infrared mode, ν_{14}, at 1220 cm^{-1} is 60% due to the rocking motion of the oxygen atom. The isotopic shifts which should be observed in the vibrational spectra upon replacement of ^{16}O by ^{18}O and of all ^{14}N's by ^{15}N's have also been calculated. The results are summarized in Table 3.

Finally, the nitrogen NMR shifts for N_7O^+ at the PBE1BPE/6-311+G(2df) level of theory have also been calculated. The following chemical shifts in parts per million relative to CH_3NO_2 are predicted: N2 = −10.2, N3 = −157.9, N5 = −164.0, and N7 = −64.8. These

Table 2. B3LYP/cc-pvtz Force Constants[a] and Potential Energy Distribution[b] of C_{2v} N_7O^+

		force constants							
symmetry class	frequency cm^{-1}	F_{11}	F_{22}	F_{33}	F_{44}	F_{55}	F_{66}	F_{77}	PED
a_1	2314	21.351	0.182	1.260	−0.478	−0.098	−0.209	0.102	$75.1S_1 + 23.8S_3$
	1559		11.249	−0.280	1.674	1.090	0.061	0.019	$51.4S_2 + 18.7S_6 + 15.5S_4 + 13.4S_5$
	1176			7.078	0.558	−0.650	1.121	0.261	$61.3S_3 + 23.0S_4$
	968				6.048	−1.001	0.881	−0.009	$44.9S_6 + 26.4S_7 + 14.2S_4$
	525					4.076	−0.275	−0.037	$86.6S_7$
	427						1.710	0.083	$79.7S_7 + 16.7S_5$
	133							0.425	$66.9S_7 + 28.3S_6$

		F_{88}	F_{99}	
a_2	504	0.125	−0.001	$98.5S_9$
	166		0.017	$76.4S_{12} + 23.5S_{11}$

		$F_{10,10}$	$F_{11,11}$	$F_{12,12}$	
b_1	703	0.785	−0.298	−0.014	$55.4S_{11} + 44.7S_{10}$
	540		0.278	0.009	$99.1S_{12}$
	94			0.018	$76.4S_{12} + 23.5S_{11}$

		$F_{13,13}$	$F_{14,14}$	$F_{15,15}$	$F_{16,16}$	$F_{17,17}$	$F_{18,18}$	
b_2	2307	21.336	1.321	−0.504	−0.186	−0.003	0.106	$75.3S_{13} + 22.8S_{14}$
	1220		6.703	0.715	1.017	−0.271	0.273	$60.1S_{17} + 28.3S_{15}$
	1008			4.446	0.852	0.451	−0.022	$82.0S_{14} + 10.5S_{17}$
	798				1.593	0.060	0.069	$43.1S_{18} + 36.6S_{16} + 10.6S_{17}$
	495					1.395	−0.005	$67.8S_{18} + 24.8S_{17}$
	225						0.419	$76.9S_{18} + 19.1S_{16}$

[a] Stretching constants in mdyn/Å, deformation constants in mdyn Å/rad^2, and stretch−bend interaction constants in mdyn/rad. [b] PED in percent. Coordinates contributing less than 10% have been omitted. Coordinates have been defined as follows (normalization factors have been omitted): $S_1 = \nu(N_5{-}N_7) + \nu(N_6{-}N_8)$, $S_2 = \nu(O{-}N_2)$, $S_3 = \nu(N_3{-}N_5) + \nu(N_4{-}N_6)$, $S_4 = \nu(N_2{-}N_3) + \nu(N_2{-}N_4)$, $S_5 = \delta(O{-}N_2{-}N_3) + \delta(O{-}N_2{-}N_4)$, $S_6 = \delta(N_2{-}N_3{-}N_5) + \delta(N_2{-}N_4{-}N_6)$, $S_7 = \delta(N_3{-}N_5{-}N_7) + \delta(N_4{-}N_6{-}N_8)$, $S_8 = \omega(O{-}N_2{-}N_3{-}N_5) + \omega(O{-}N_2{-}N_4{-}N_6)$, $S_9 = \omega(N_2{-}N_3{-}N_5{-}N_7) + \omega(N_2{-}N_4{-}N_6{-}N_8)$, $S_{10} = \omega(O{-}N_2{-}N_3{-}N_4)$, $S_{11} = \omega(O{-}N_2{-}N_3{-}N_5) - \omega(O{-}N_2{-}N_4{-}N_6)$, $S_{12} = \omega(N_2{-}N_3{-}N_5{-}N_7) - \omega(N_2{-}N_4{-}N_6{-}N_8)$, $S_{13} = \nu(N_5{-}N_7) - \nu(N_6{-}N_8)$, $S_{14} = \nu(N_3{-}N_5) - \nu(N_4{-}N_6)$, $S_{15} = \nu(N_2{-}N_3) - \nu(N_2{-}N_4)$, $S_{16} = \delta(N_2{-}N_3{-}N_5) - \delta(N_2{-}N_4{-}N_6)$, $S_{17} = \delta(O{-}N_2{-}N_3) - \delta(O{-}N_2{-}N_4)$, $S_{18} = \delta(N_3{-}N_5{-}N_7) - \delta(N_4{-}N_6{-}N_8)$.

Table 3. ^{18}O and ^{15}N Isotopic Shifts (cm^{-1}) of C_{2v} N_7O^+ at the B3LYP/cc-pvtz Level

$^{16}O{-}^{14}N$	$^{18}O{-}^{14}N$	$^{16}O{-}^{15}N$	$^{18}O{-}^{15}N$	$(^{18}O{-}^{14}N) - (^{16}O{-}^{14}N)$	$(^{16}O{-}^{15}N) - (^{16}O{-}^{14}N)$	$(^{18}O{-}^{15}N) - (^{16}O{-}^{14}N)$
2314.0	2314.0	2235.6	2235.6	0.0	−78.4	−78.4
2307.7	2307.7	2229.5	2229.5	0.0	−78.2	−78.2
1558.9	1525.9	1526.9	1492.3	−33.0	−32.0	−66.6
1220.2	1218.2	1180.1	1178.0	−2.0	−40.1	−42.2
1176.2	1175.2	1136.9	1135.9	−1.0	−39.3	−40.3
1007.9	1007.4	974.0	973.5	−0.5	−33.9	−34.4
968.0	955.1	942.2	930.1	−12.9	−25.8	−37.9
798.1	795.4	772.7	769.9	−2.7	−25.4	−28.2
703.2	698.9	682.0	677.6	−4.3	−21.2	−25.6
539.6	539.5	521.3	521.2	−0.1	−18.3	−18.4
525.2	524.7	507.8	507.2	−0.5	−17.4	−18.0
504.5	504.5	487.4	487.4	0.0	−17.1	−17.1
494.9	483.7	484.8	473.5	−11.2	−10.1	−21.4
427.4	424.0	414.7	411.6	−3.4	−12.7	−15.8
225.3	221.1	220.1	216.0	−4.2	−5.2	−9.3
166.4	166.4	160.8	160.8	0.0	−5.6	−5.6
133.9	133.1	129.7	129.0	−0.8	−4.2	−4.9
93.7	92.3	91.4	90.0	−1.4	−2.3	−3.7

data will facilitate future experimental searches for this interesting cation.

Since all attempts to isolate N_7O^+ had been unsuccessful while N_3NOF^+ possesses good thermal stability, the question arose whether this was due to a poor choice of reagents or reaction conditions or if there is a general innate stability problem with geminal diazides. In order to deal with this problem, it is imperative to understand the decomposition mechanism of N_7O^+ and *gem*-diazides in general.

In the study of the decomposition of N_7O^+, five different pathways were found with transition states (TS) which are illustrated in Figure 3 and with relative energies summarized in Figure 4. Intrinsic reaction coordinate calculations were performed to trace the minimum energy pathway from each transition state to reactants and products. Two of the five transition states originate from the C_{2v} ground state and involve the interaction of the negatively charged oxygen atom with

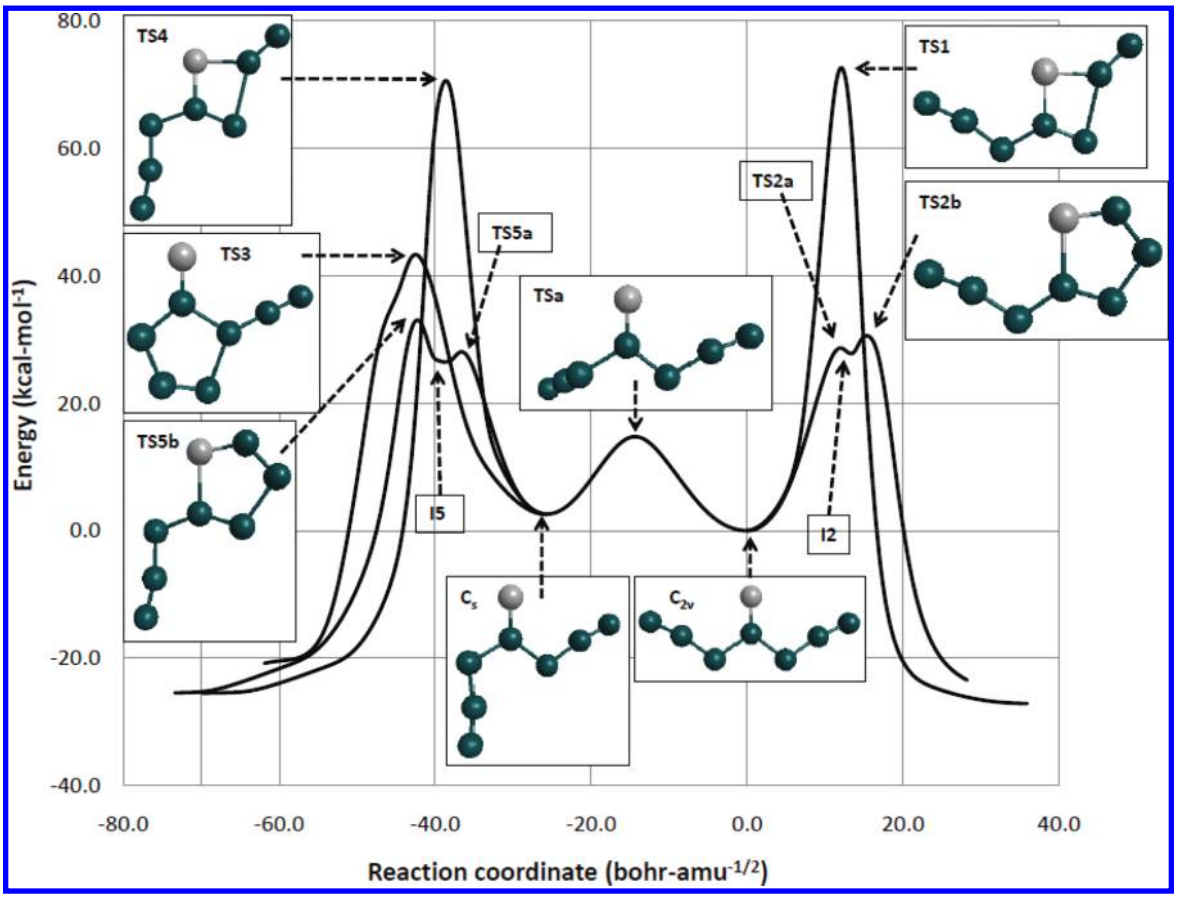

Figure 3. B3LYP/6-311G(2df) intrinsic reaction coordinate traces (solid curves) and stationary points for the decomposition reaction of N_7O^+. Oxygen (nitrogen) atoms are shown as light (dark) circles. Local minimum I2 is identical to the cyclic isomer shown in Figure 2.

either a positively charged Nβ atom of an azido group, resulting in a four-membered ring (TS 1), or an also positively charged Nγ atom, resulting in a five-membered ring (TS 2). (The NBO charge distributions of N_7O^+ are given in the diagram caption of Figure 1.) Note that, in the case of TS 2, the decomposition pathway is actually a two-step process that goes through a cyclic intermediate I2, which is the same as the cyclic structure shown in Figure 2. The transition state structures preceding (TS2a) and following (TS2b) the formation of I2 are nearly identical in structure and relative energy, and therefore only TS2b is shown in Figure 3.

Since the energy difference between the C_{2v} and the C_s structure is only ~3 kcal/mol with a low interconversion barrier of ~14 kcal/mol, a possible decomposition mechanism starting from the C_s state was also explored. Again, there can be an interaction between the O atom with either Nβ (TS 4) or Nγ (TS 5) of that azido group, which points in the same direction as the oxygen. Similar to the TS 2 reaction pathway discussed previously, the TS 5 decomposition pathway is actually a two-step process going through a cyclic intermediate I5, preceded and followed by TS5a and TS5b, respectively. The TS5a, TS5b, and I5 stationary points are nearly identical in structure and relative energy, and therefore only TS5b is illustrated in Figure 3. An additional decomposition pathway involves the interaction between the positively charged Nγ atom of the azido group pointing away from the oxygen atom, with the negatively charged Nα atom of the azido group pointing in the same direction as the oxygen atom (TS 3). The calculated barriers are shown in Figures 3 and 4. As can be seen, the barriers involving four-membered cyclic transition states are ~70 kcal/mol and are much higher than those involving five-membered rings and, therefore, can be discounted.

To further discriminate between the different decomposition mechanisms, we have also carried out decomposition studies using ^{15}N labels. For this purpose, we have prepared labeled N_7O^+ with partial ^{15}N labels in the Nα and the Nγ positions, using the singly, terminally labeled azide ion as the starting material (eq 5).

$$2[N{-}N{-}*N]^- \rightarrow H{-}*N\alpha{-}N\beta{-}N\ \gamma + H{-}N\alpha{-}N\beta{-}*N\gamma \rightarrow [*N\ \gamma{-}N\beta{-}*N\alpha{-}N(O){-}*N\alpha{-}N\beta{-}*N\gamma]^+ \quad (5)$$

The distribution of the ^{15}N labels in the N_7O^+ decomposition products was determined by ^{15}N NMR spectroscopy. It was found that the N_2O was exclusively labeled on the terminal N, that is, *N−N−O, and that in N_5^+ the ^{15}N label was equally distributed over all five positions. Of the five different mechanisms studied by us, only the mechanism TS 3 involving the attack of the positively charged Nγ atom of the azido group pointing away from the oxygen atom on the negatively charged Nα atom of the azido group pointing in the same direction as the oxygen atom can account for the observed distribution of the ^{15}N labels (Figure 5) and has a reasonably low activation barrier (~42 kcal/mol), which is about half of that predicted for N_3NOF^+ (~80 kcal/mol). Although all of these barriers

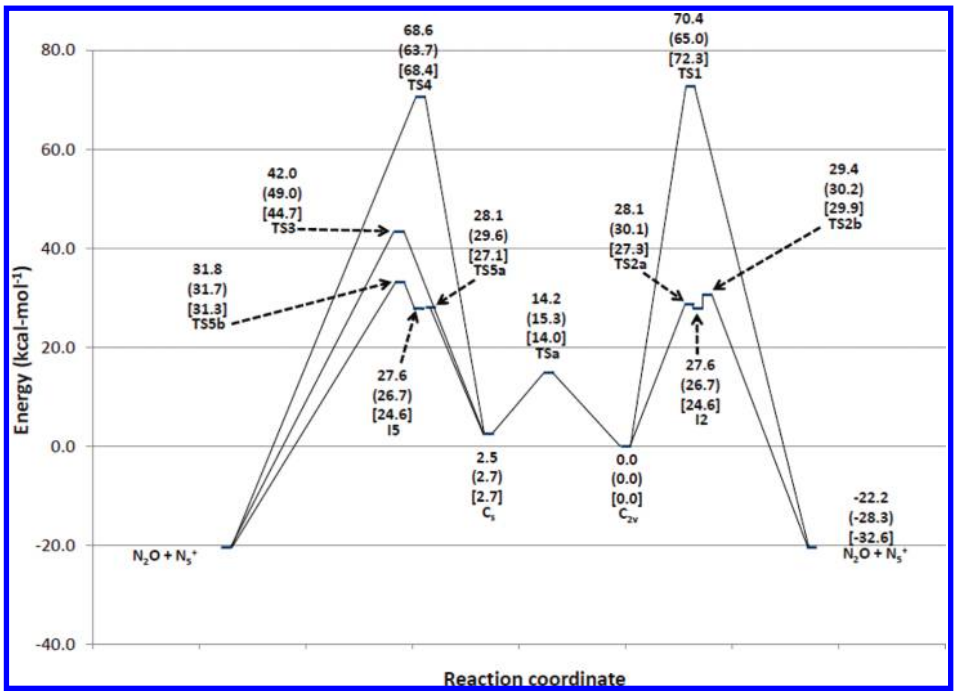

Figure 4. Relative energies (kcal/mol), at the B3LYP/6-311G(2df) level of theory, including scaled B3LYP zero-point vibrational energy corrections. MP2/6-311G(2df) and CR-CCSD(T)/cc-pvtz//MP2/6-311G(2df) values, both of which include scaled MP2 zero-point vibrational energies, are shown in parentheses and brackets, respectively.

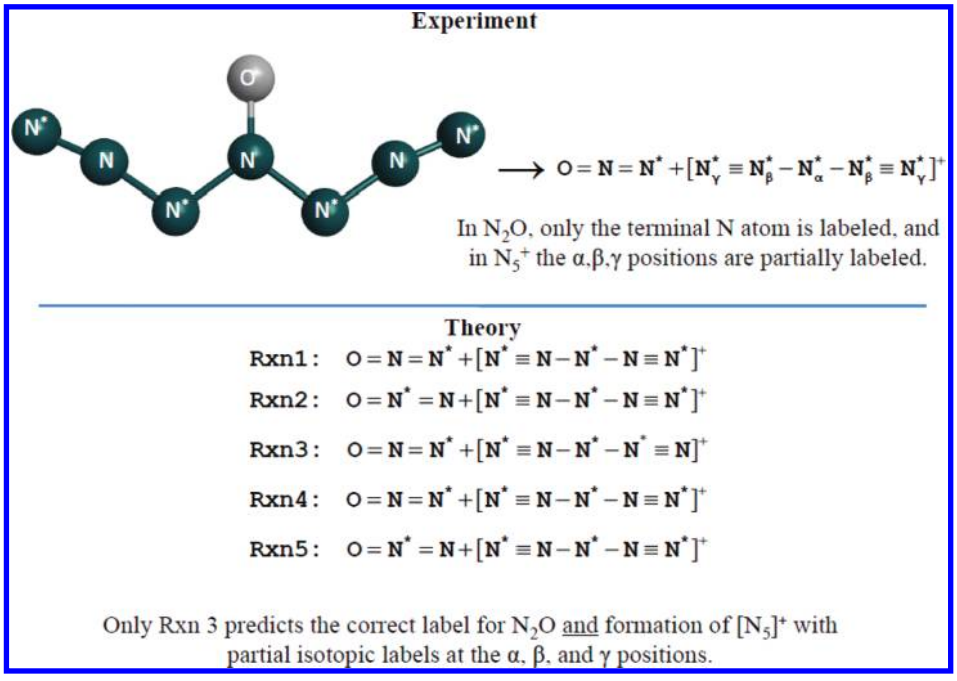

Figure 5. Comparison of the theoretically predicted and the experimentally found ^{15}N labels in the decomposition products of N_7O^+.

are higher than expected, it is possible that the calculations overestimate the size of the barriers or that the barriers in solution are considerably lower than in the free gas phase. Nevertheless, this study clearly demonstrates that the diazido N_7O^+ cation has a much lower barrier than the monoazido N_3NOF^+ cation, in excellent agreement with the experimental observations. Furthermore, the fact that the preferred mechanism requires the presence of two geminal azido ligands explains the general observation in azide chemistry that geminal diazides are much more sensitive and unstable than either monoazides or vicinal diazides. The inadvertent formation of geminal diazides as a byproduct in the synthesis of monoazides has led in the past to severe accidents and injuries and must be avoided under all circumstances. These conditions apply not only to azide substituted amine oxides but are equally valid for azidamines and other similar compounds, the only difference being the nature of the elimination product. In the case of multiply azide substituted amines, the elimination product becomes N_2

instead of N_2O, but the decomposition mechanism remains the same.

Conclusions

The N_7O^+ cation was prepared from the low-temperature reaction of NOF_2^+ with a 2-fold excess of HN_3 in anhydrous HF solution. The N_7O^+ cation is thermally very unstable and decomposes instantaneously to N_5^+ and N_2O, thus preventing its direct observation. However, its formation was well established by NMR spectroscopy of the decomposition products, by the use of ^{15}N labeling, and by the results from a theoretical study. The decomposition mechanism of N_7O^+ was analyzed and involves the electrophilic attack of the terminal γ-N atom of one azide ligand on the electron-rich α-N atom of the second azide ligand, thus explaining the generally observed instability of geminal diazides.

Acknowledgment. This work was funded by the Air Force Office of Scientific Research, the Office of Naval Research, the Defense Threat Reduction Agency, and the National Science Foundation. Any opinions, findings, and conclusions or recommendations expressed in this material are those of the authors and do not necessarily reflect the views of the National Science Foundation.